Thermophysical properties and containerless solidification of Al-22.5wt%Cu in reduced gravity using the ISS-EML

Q.Champdoizeau[1], J.Valloton[1a], H.Henein[1]

[1]University of Alberta, Edmonton, Canada
[a]valloton@ualberta.ca

Keywords: Aluminum Copper, Thermophysical properties, Solidification, ISS-EML

Abstract

A hypoeutectic Al-22.5wt%Cu sample was processed using the Electro-Magnetic Levitator on board of the International Space Station within the frame of the European Space Agency project NEQUISOL and THERMOLAB. In total, 21 cycles of melting and cooling were carried out, with the last cycle yielding a primary undercooling of 20 K and a eutectic undercooling of 35 K. The density, surface tension, and viscosity of the sample were measured using the oscillating drop method and a high-speed camera. The evolution of the temperature was recorded with a pyrometer. The oscillations of the drop appear modulated, indicative of a nonlinear behavior caused by rotation, precession, nutation of the sample, and high initial deformation. After being returned to Earth, preliminary investigation of the surface of the sample showed unexpected features. The growth direction of the visible dendrites seemed to differ from the characteristic ⟨100⟩ expected of primary α-Al. Furthermore, two distinct eutectic morphologies were observed: a typical lamellar eutectic, as well as an undulated structure, akin to what is formed in rapidly solidified eutectic Al-33wt%Cu droplets.

Introduction

The optimization of high temperature metallurgical processes such as atomization, welding or casting requires building numerical models using the thermophysical properties of metallic liquids as inputs. The development of an accurate database for the density, gas-liquid surface tension, and viscosity of metals and alloys is then essential to understand and analyze the physics of these processes [1]. The THERMOLAB project aims at measuring these thermophysical properties, in weightlessness conditions, for samples processed in the Electromagnetic Levitator onboard of the International Space Station (ISS-EML) [2]. In this work, the microstructure and thermophysical properties of hypoeutectic Al-22.5wt%Cu are investigated through containerless melting and solidification cycles carried out using the ISS-EML equipment. First, the method to process the sample will be described, followed by the presentation of the results for the measurements of the density, surface tension, and viscosity. A discussion of the undercooled solidified microstructure will finally be presented.

Experimental Method

Electromagnetic levitation (EML) is a powerful solidification and thermophysical property measurement technique for analysis of electrically conducting samples such as metals and semiconductors. By avoiding contact with any container walls and operating under high purity environment, heterogeneous nucleation is strongly reduced and a large range of undercoolings can be achieved. In EML, the sample is placed within a conical levitation coil typically consisting of five to seven water-cooled copper windings with one or two counterwindings at its top as shown in Fig.1.

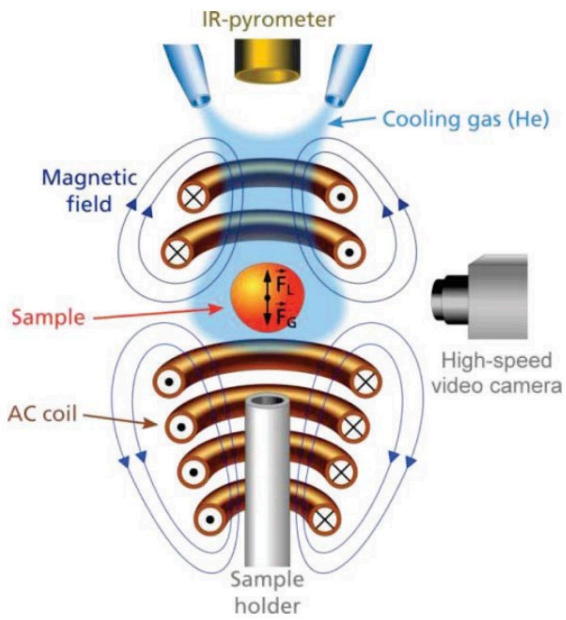

Figure 1. Schematic of EML, taken from [3]

Eddy currents are induced in the sample by the electromagnetic field generated by the levitation coils. The sample is heated and melted by ohmic losses, whereas the interaction of these eddy currents with the electromagnetic field leads to a displacement force on the sample that is opposite to the gravitational force. The temperature of the sample is monitored continuously with a contactless pyrometer. To cool the sample below its liquidus temperature and induce solidification, a jet of high purity helium is used. Detailed information on the EML technique can be found in [4]. A radial camera with a frame rate of 100 Hz is looking from the side of the sample with a window of 10x10 cm or 608x608 pixels. This camera is combined with a pyrometer for temperature measurements. The Al-22.5%wtCu sample was made from high purity Al-6N and Cu-6N and had a mass of m = 439.870 mg and a diameter around 6.4 mm. In total, 21 cycles of melting and solidification were performed during the ISS experiments. The sample is assumed to be oxygen saturated. An oxide layer was always observed at the start of melting, disappearing when reaching high enough temperatures and reforming at the end of the cooling cycles. The data was trimmed of the end part when the oxide layer was visibly forming again as it would impact the surface tension measurement. For each cycle, the available dataset consists of the combination of the video recorded by the radial camera and the temperature profile measured by the pyrometer. The density, ρ, the surface tension, σ, and the viscosity, η, of the sample are estimated using the oscillating drop technique [5]. The oscillations of the sample are triggered by a short pulse stretching the drop along the heating field and resulting in damped surface oscillations until reaching the equilibrium spherical shape. A cycle typically takes around 2 minutes and the total mass loss for the sample was 0.760mg after all the cycles. The droplet oscillations were monitored by the radial video camera and the images were first analyzed using a dedicated software “TeVi” (SEA Datentechnik GmbH), which detects the edges of the sample from the image contrast as well as the horizontal and vertical radii, R_x and R_y, as shown in Fig.2.a. However, the strong initial deformation causes the sample to rotate around a varying axis and translate which leads to inconsistent oscillations. Fig.2.b and Fig.2.c show that the oscillations appear really scattered between the horizontal and vertical radius. The evolution of both radius are shown in number of pixels as a function of the number of seconds since the pyrometer was started.

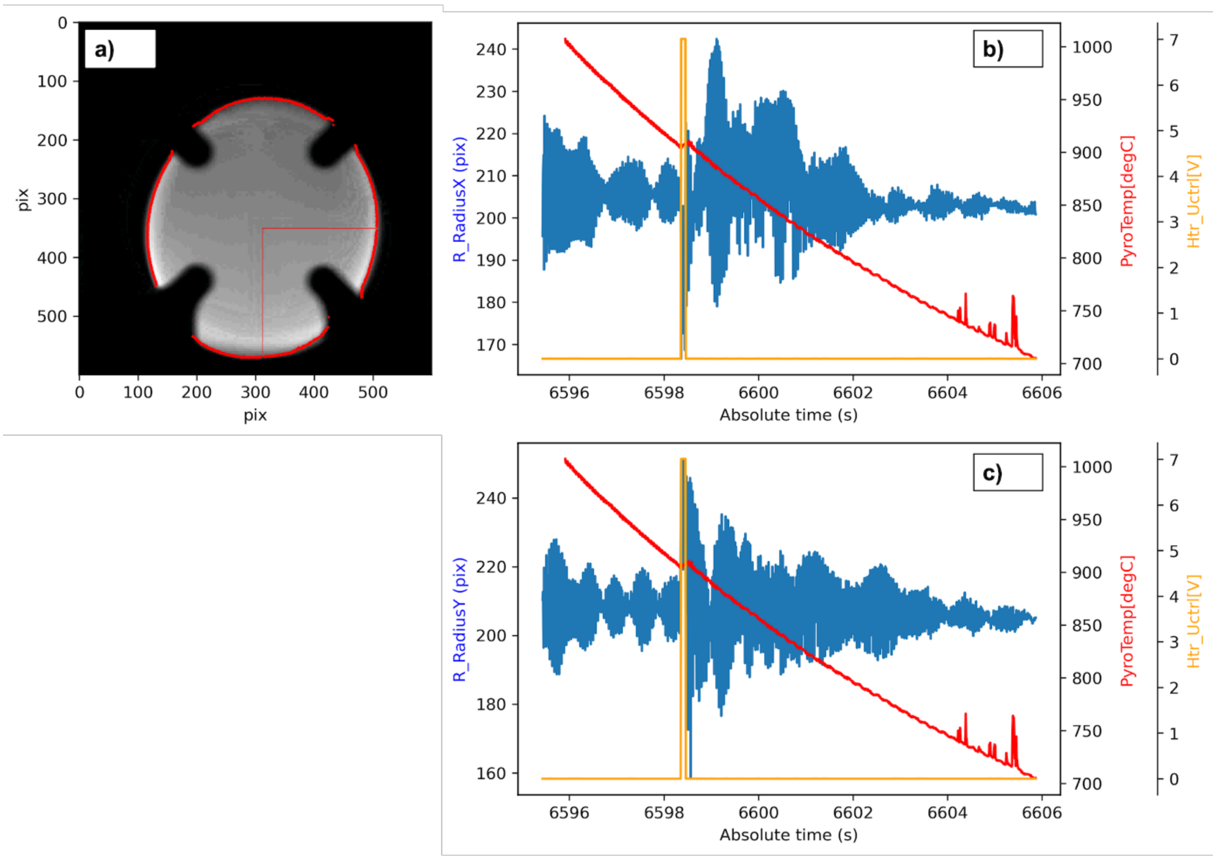

Figure 2. Cycle 14 a): Frame at t=3.08s after pulse. b) Oscillations of R_x. c) Oscillations of R_y

It was then chosen to fit an elliptical profile to the detected edges of the sample and measure a and b, the minor and major axes of the sample, for each time frame. An example of this process can be seen in Fig.3, with the elliptical profile shown in white.

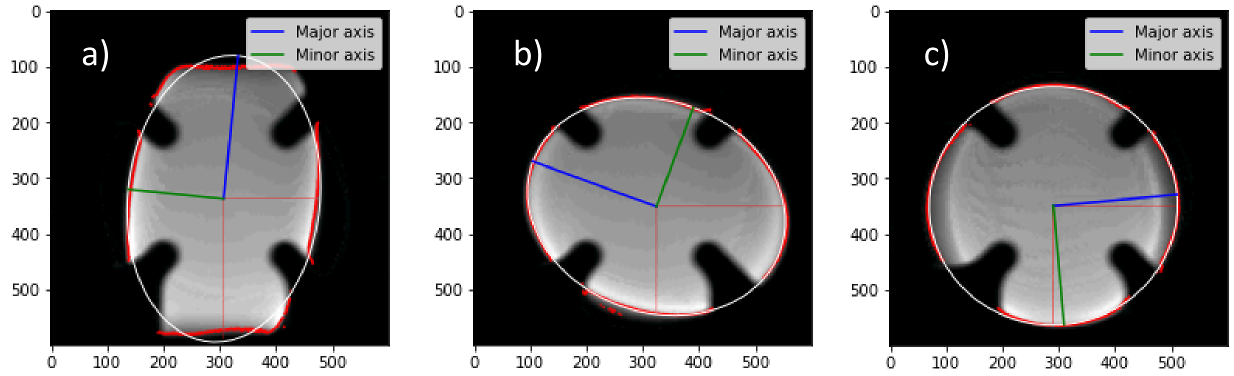

Figure 3. Cycle 14 a): Frame at t=0.00s after pulse. b) t= 1.45s after pulse. c) t=4.78s after pulse

It is then possible to apply the oscillating drop method using four different radii, R_x, R_y, a and b, to calculate the thermophysical properties. The effective radius R_{eff} is then introduced as $R_{eff} = \sqrt{ab}$ to minimize the scatter caused by the overlap between the rotation and translation of the sample and its oscillations [6]. After Fast Fourier Analysis of the oscillations, a high pass filter at 30 Hz was applied to eliminate the background noise and reveal the relative damped oscillations as shown in Fig.4. The calculations of the uncertainties for the three properties have been conducted according to the Evaluation of Measurement Data-Guide to the Expression of Uncertainty in Measurement principal handbook while assuming the sources of errors to be independent [7].

The surface of the sample was observed using a Tescan Vega scanning electron microscope. Images of the microstructure were acquired with an acceleration voltage of 20 kV and a working distance of 10 mm using the backscatter electron detector.

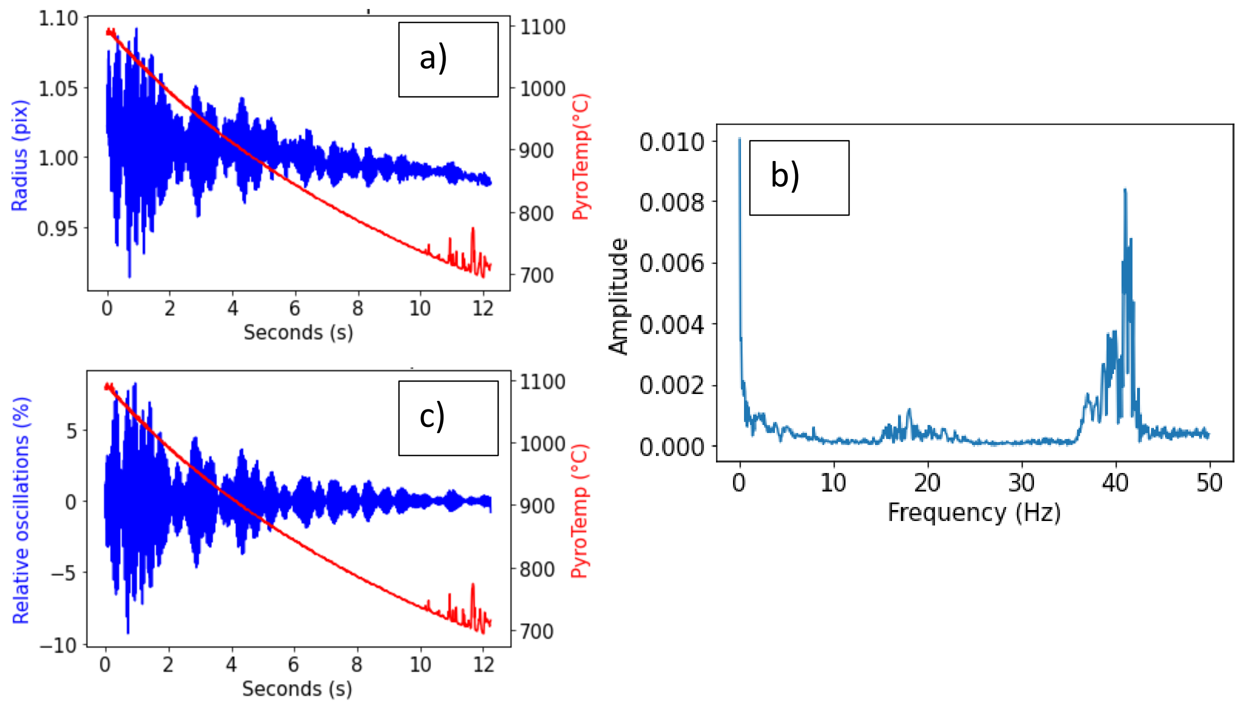

Figure 4. Cycle 11 a) Before filtering b) Fast Fourier Transform of the oscillations c) After High-pass 30Hz filtering

Results and Discussion

Density

The density of the sample can be calculated as $\rho(T) = \frac{m}{V(T)}$ with m and V the mass and volume of the sample respectively. The volume is traditionally calculated by fitting Legendre polynomials to the detected edges of the sample to determine the radius profile $R(\theta)$ of the drop, with θ the angle from the horizontal axis. By assuming a vertical axis of symmetry for the rotation, the volume can then be calculated from $V = \frac{2}{3}\pi \int_0^\pi R(\theta)^3 \sin(\theta)\, d\theta$. However, the strong deformations and the coils hide part of the edges of the drop making the volume to be underestimated with this method. Instead, we approximated the volume of the sample by assuming its shape to be described by an ellipsoid symmetrical along its major axis, also called a spheroid, such as $V = \frac{4}{3}\pi a^2 b$. Other modes of oscillations can arise from the initial strong deformation leading to nonlinearities and invalidating the spheroidal shape assumption for the drop. The beginning of the oscillations is then trimmed so that the relative oscillations are under 5% to get more accurate measurements of the density in the domains where the oscillations are linear. The density measurements are averaged in segments where the temperature drops by 10°C which leads to 10-15 measurements per cycle. In Fig.5, the results of this study for the density of Al-22.5wt%Cu are presented alongside with the Ideal solution model and experimental results obtained using the Gas Bubble Pressure method and the Oscillating Vessel method [8-9]. The results agree especially well with the ideal solution predictions. The increased scattering of the results obtained in this study at the highest temperatures is understood to be caused by the residual nonlinearities affecting the spheroidicity of the drop and the precision of the edge detection algorithms.

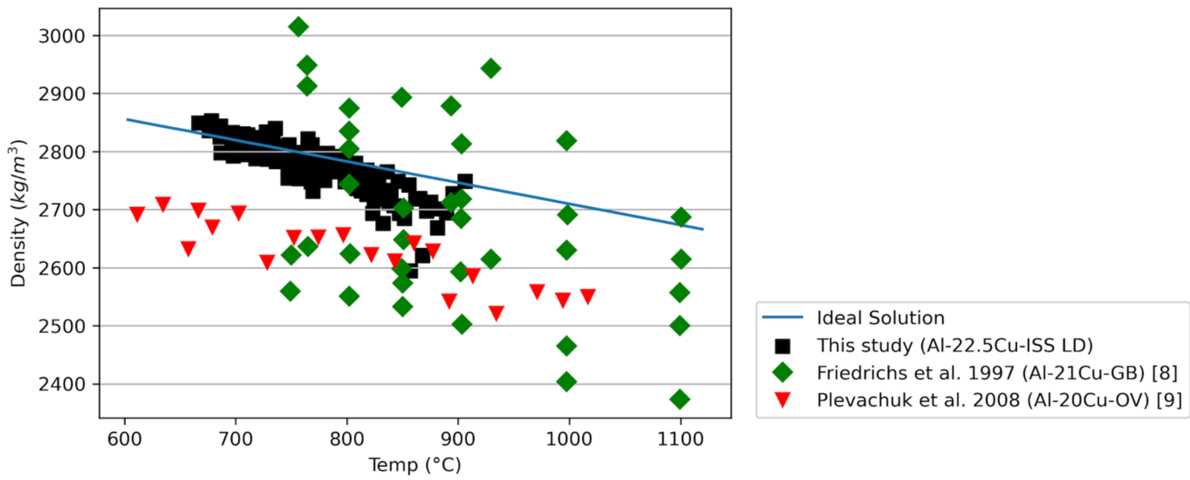

Figure 5. Density results

Surface tension

During the oscillations, the shape of the drop can be described mathematically using spherical harmonics [10]. In microgravity the oscillations modes are degenerated and so assume the same frequency while the second mode of oscillation is the most stable and the dominating one. Under the linear assumption of small amplitude oscillations, Rayleigh derived the relationship between the surface tension of the fluid and the natural frequency of the oscillations f_n, and the mass of the sample such as $\sigma(T) = \frac{3\pi m f_n(T)^2}{8}$ [11]. The natural frequency can be determined as the maximum peak frequency of a Fast Fourier Transform (FFT) of the oscillation’s amplitude. The uncertainty on the measurement of the natural frequency from the FFT is inversely proportional to the signal duration. Inversely, the uncertainty on the temperature is proportional to the signal duration as the temperature drops during the oscillations. An optimal condition is found for a signal duration between two and three seconds. For the analysis, the oscillations of each cycle are then segmented into two-second-long portions. This allows for multiple surface tension measurements per cycle while the temperature decreases. In Fig.6, the results of this study for the surface tension are compared with the Butler model and experimental results obtained using the Gas Bubble Pressure method, the Levitated Drop method and the Discharge Crucible method [8, 12-14]. The measurements obtained in this study are consistent with the results predicted by the Butler model [12] and the experimental results obtained by P.Flood [13] and Shmitz et al. [14]. The limited resolution of 0.5 Hz of the FFT for two-second long segments of data recorded at an acquisition rate of 100 Hz is limiting the precision in the identification of the maximum peak frequency. Additionally, the rotation of the droplet and the nonlinear deformation may cause splitting of the resonance peak and frequency shift [15].

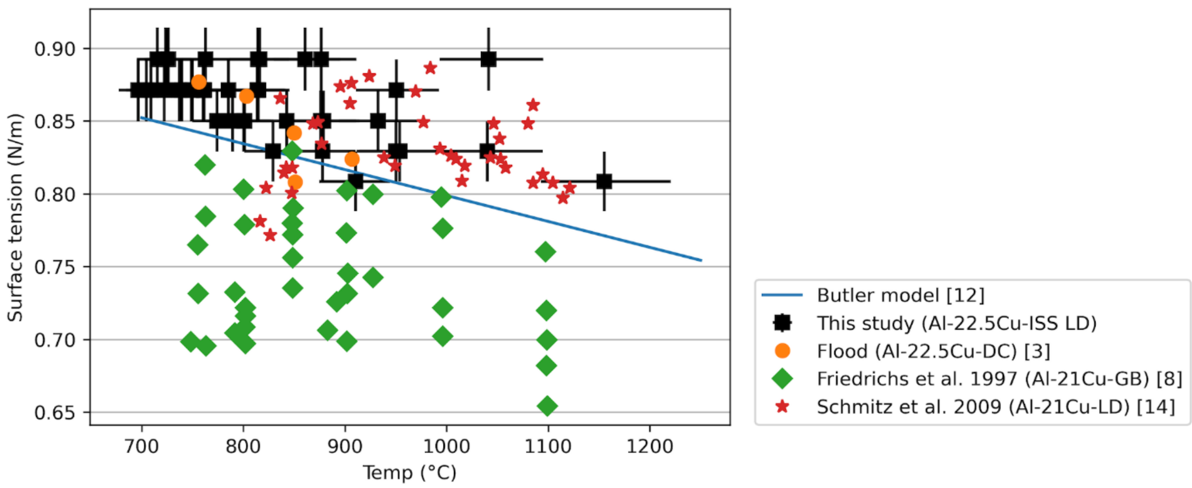

Figure 6. Results for surface tension

Viscosity

The viscosity is related to the damping constant τ of the oscillations according to the Lamb equation such as $\eta(T) = \frac{3m}{20\pi R_o(T)\tau(T)}$ [16]. The effective radius oscillations seem modulated suggesting strong nonlinearities at play as shown in Fig.3 and Fig.4. As a result, significant information on the evolution of the peaks of the amplitude is missing which prevents from accurately fitting an exponential decay envelope to segments of the signal to determine the decay constant and thus, the viscosity. To minimize the uncertainty, this fitting is then done on selected peaks of the whole data set from the initial deformation as opposed to the segmented analysis for the surface tension. Fig.7 show a result of this fitting executed on the lower and upper envelope.

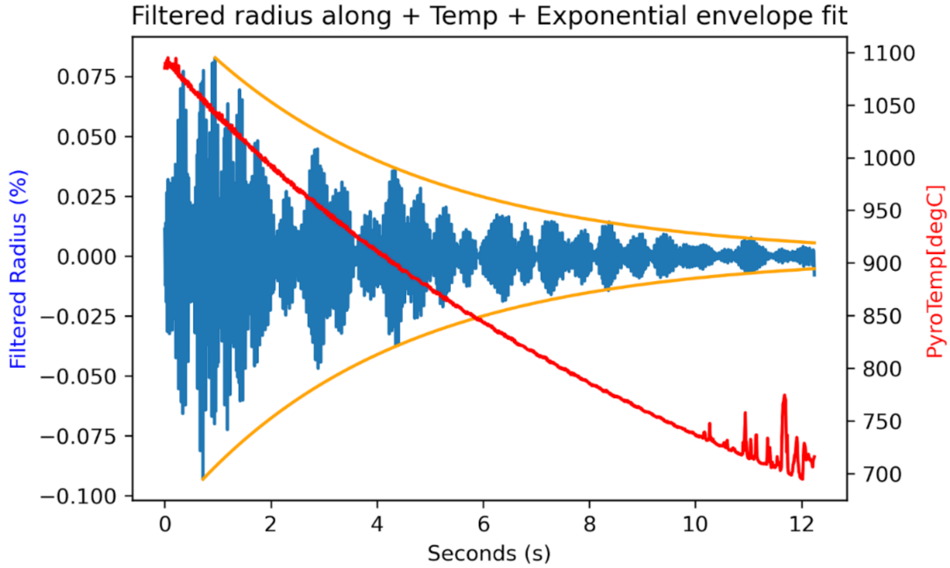

Figure 7. Cycle 11) Exponential fitting of the envelope of the relative oscillations of the effective radius.

In Fig.8, the results of this study for the viscosity of Al-22.5wt%Cu are compared with experimental results obtained using the Gas Bubble Pressure method, the Oscillating Vessel method, and the Discharge Crucible method [8,13,17-18]. The measurements are agreeing well with the experimental results by P.Flood [13], Schick et al. [17] and Konstatinova [18]. The uncertainties on the measurements are understood to be due to the high initial deformation giving rise to nonlinear oscillations. This phenomenon coupled with the sample rotation and translation modulate the perceived damped oscillations from the side camera point of view and affect the precision of the Lamb equation in predicting the viscosity of the sample. More research is needed to consider the nonlinearities arising from initial high deformation and leading to the temporary presence of other modes of oscillations to correct the lamb equation and modify the modelling of the damped oscillations [19].

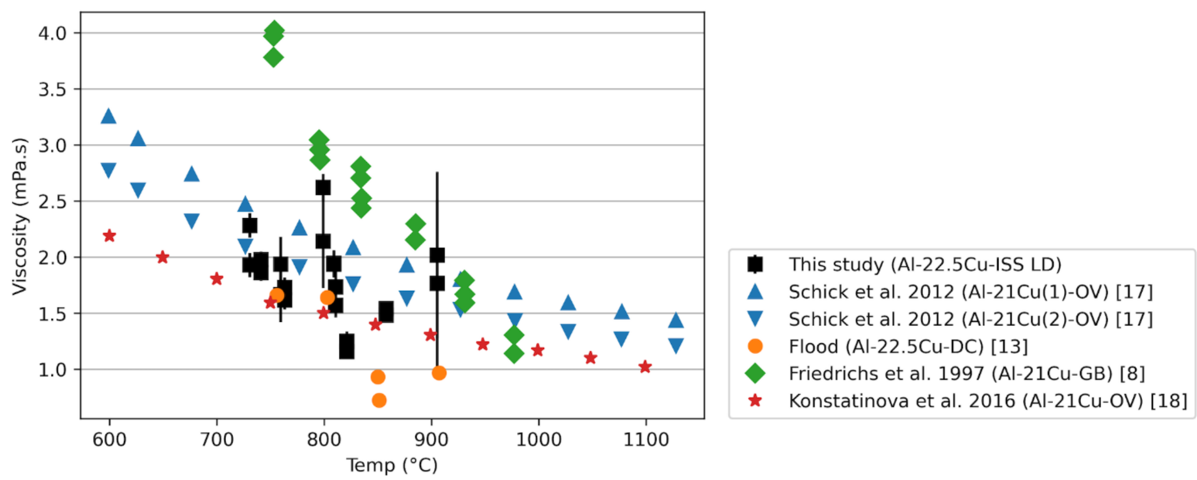

Figure 8. Viscosity results

Microstructure

Figure 9 shows the temperature-time profile of the last solidification cycle performed on the Al-22.5wt%Cu sample. Two recalescence events are observed. The first one corresponds to the primary nucleation of α-Al, with an undercooling of $\Delta T_{primary}$ = 23 K. The second event is the nucleation of the α-Al-Al_2Cu eutectic with and undercooling of $\Delta T_{eutectic}$ = 35 K.

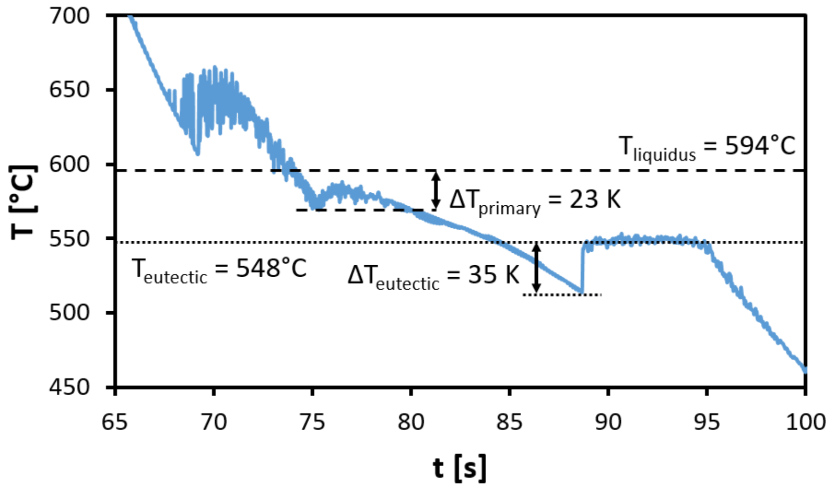

Figure 9. Cycle 21) Temperature-time profile of the last solidification cycle.

Due to the uniqueness and rarity of this sample, it is important to perform a complete characterization, which starts with non-destructive techniques. At the time of writing, the sample was at Los Alamos National Laboratory to undergo neutron diffraction, which will be followed by synchrotron X-ray tomography at the Canadian Light Source. Microstructure analysis is thus far limited to the surface of the sample. Figure 10 shows an SEM micrograph of the region that solidified last. A large amount of porosity due to solidification shrinkage can be seen. The dendrites present are well developed. However, their morphology is reminiscent of seaweed. They do not exhibit the 4-fold symmetry typical of the ⟨100⟩ of α-Al. None of the primary dendrites visible at the surface of the sample seem to grow along ⟨100⟩. Deviation from ⟨100⟩ growth direction in Al-Cu alloys has been previously reported. α-Al dendrites have been shown to grow along ⟨111⟩ directions in impulse atomized Al-4.5wt%Cu [20-21]. This has been attributed to the anisotropy of attachment kinetics. However, the cooling rates and undercoolings involved in atomization are much higher than what was experienced by the Al-22.5wt%Cu sample in the MSL-EML. This deviation is perplexing as both Al and Cu have interfacial energy anisotropies that favour ⟨100⟩ growth. This will be investigated further with X-ray tomography and the following full metallographic study of the sample.

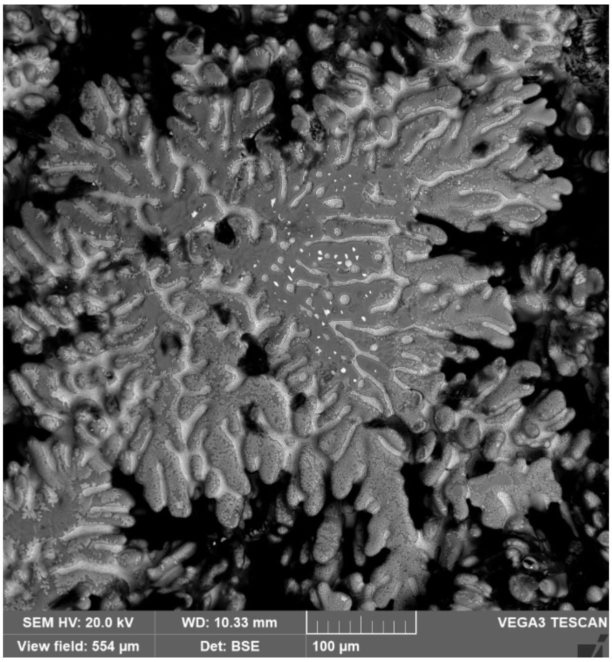

Figure 10. SEM micrograph of the end of solidification.

Figure 11 shows a close-up of the microstructure on the opposite side of Figure 8. As expected, it is composed of primary α-Al surrounded by an α-Al-Al_2Cu eutectic. However, two distinct morphologies are observed. Figure 8 left displays a typical lamellar eutectic, while the eutectic in Figure 8 right can be defined as undulated. Such a morphology has been observed in rapidly solidified eutectic Al-33wt%Cu droplets [22]. It is assumed that the undulated eutectic grows rapidly during recalescence, while the lamellar eutectic grows post-recalescence during the eutectic plateau. Since the eutectic undercooling is fairly small (35 K), the amount of undulated eutectic should be much less than that of the lamellar. This will be further explored during the metallographic analysis of the sample.

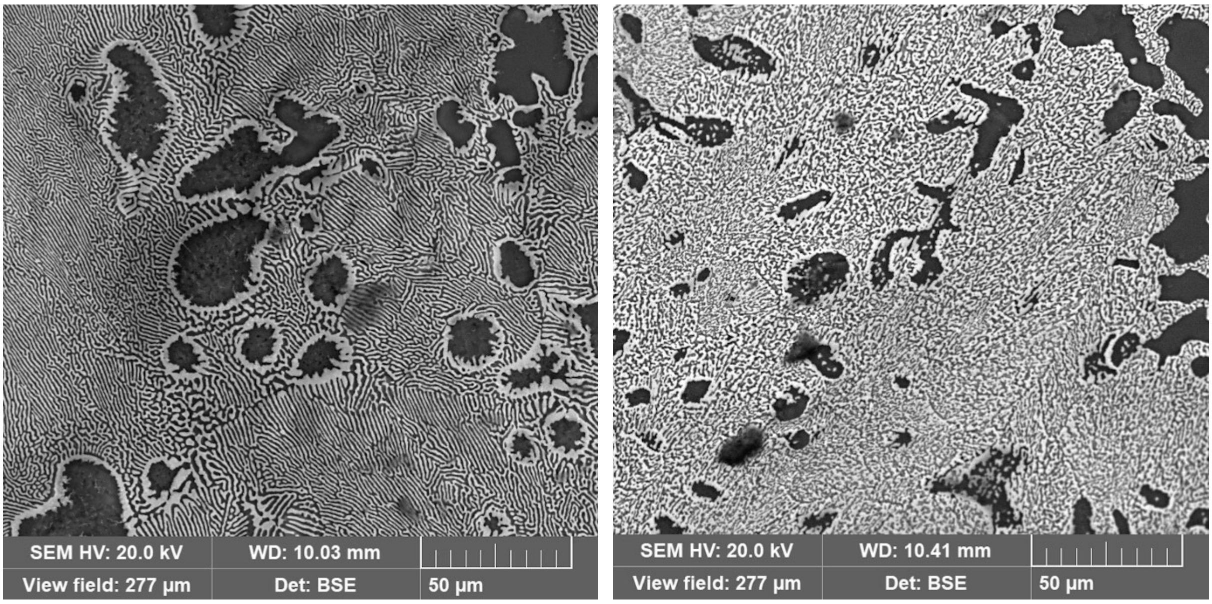

Figure 11. Two different eutectic morphologies observed at the surface of the Al-22.5wt%Cu sample: regular lamellar (left) and undulated (right).

Conclusions

Overall, the measurements obtained for the density, surface tension and viscosity of the Al-22.5wt%Cu sample with the Oscillating Drop Method applied on data obtained from the ISS-EML are consistent with results in the literature. However, the low weight of the sample made it difficult to constrain the initial deformation to a linear regime. The only available images were taken from the side camera and were showing a nonlinear behavior for the damped oscillations coupled with rotation and translation of the sample. This affected the precision of the method for the calculation of the three thermophysical properties. The shape of the sample was likely non spheroidal at the beginning due to the presence of higher modes of oscillations than the assumed second mode. This nonlinear regime was avoided for density calculation as it would lead to uncertainties. The rotation and nonlinearities also lead to peak splitting and frequency shifting in the FFT contributing to the uncertainty of the surface tension measurement. Finally, the viscosity measurement of the sample was the most affected by the nonlinear behavior. The oscillations were appearing modulated leading to an important loss of information on their amplitude and making a segmented exponential fitting of the envelope non accurate. The decay constant was then obtained through fitting of the envelope on selected peaks for the whole data available for each cycle to minimize the uncertainties and the Lamb equation was then applied to calculate the viscosity. Further research is needed to develop corrections on the traditional Rayleigh and Lamb equation [9,14] and compensate for the information loss on the perceived damped oscillations due to the rotation, translation and nonlinearities.

Preliminary investigation of the surface of the sample showed unexpected features. The growth direction of the visible dendrites seemed to deviate from the characteristic ⟨100⟩ expected of primary α-Al. Furthermore, two distinct eutectic morphologies were observed: a typical lamellar eutectic, as well as an undulated structure, akin to what is formed in rapidly solidified eutectic Al-33wt%Cu droplets. A full microstructural study will be carried out after the sample has undergone a full set of non-destructive analysis.

Acknowledgments

The authors acknowledge the access to the ISS-EML, which is a joint undertaking of the European Space Agency (ESA) and the DLR Space Administration. The reported work was conducted in the framework of the ESA research projects NEQUISOL (AO-2009-0829) and THERMOLAB (AO-2009-1020). The authors are grateful to the people at the user-support and operations centre MUSC for guiding the experimental work and for their expert support. The authors are also grateful to Dr. Douglas Matson and Dr. Jannatun Nawer for their assistance with the data analysis of this work.

References

[1] A. J. Yule and J. J. Dunkley: *Atomization of melts: for powder production and spray deposition*. Oxford University Press, USA, 1994.

[2] Soellner W., Aicher W.: *Metallurgy in Space: Recent Results from ISS*, eds. Fecht H.-J., Mohr M., Springer, Cham, 2022, pp. 25–41.

[3] Valloton, J., Herlach, D.M., Henein, H. and Sediako, D.: *Metall Mater Trans A*, 2017, 48, pp. 4735–4743.

[4] D. M. Herlach: *Solidification of Containerless Undercooled Melts*, eds. D. M. Herlach and D. M. Matson, Wiley-VCH, Weinheim, 2012, pp. 9–16.

[5] Seidel, A., Soellner, W. and Stenzel, C.: *J. Phys. Conf. Ser.*, 2011, 327, 012057.

[6] Luo, Y., Damaschke, B., Lohöfer, G., and Samwer, K.: *npj Microgravity*, 2020, *6*(1), pp. 1-9.

[7] JCGM/WG1: *Evaluation of measurement data - Guide to the expression of uncertainty in measurement*, JCGM - Joint Committee for Guides in Metrology, 2008.

[8] H. A. Friedrichs, L. W. Ronkow, and Y. Zhou: *Steel Res*., 1997, 68(5), pp. 209–214.

[9] Y. Plevachuk, V. Sklyarchuk, A. Yakymovych, S. Eckert, B. Willers and K. Eigenfeld: *Metall. Mater. Trans. A*, 2008, 39A(12), pp. 3040–3045.

[10] Mohr, M. and Fecht, H. J: *Metallurgy in Space: Recent Results from ISS*, Springer, Cham, 2022, pp. 263-280.

[11] F.R.S. Rayleigh: *Proc. R. Soc.*, 1879, 29, pp. 71–97.

[12] J. A. V. Butler: *Proc. R. Soc. London. Ser. A*, 1932, 135(827), pp. 348–375.

[13] P. Flood: *Thermophysical Properties Measurement of Liquid Al and Al-Cu by the Discharge Crucible Method*, 2020, MSc Thesis, University of Alberta.

[14] J. Schmitz, J. Brillo, I. Egry, and R. Schmid-Fetzer: *Int. J. Mater. Res.*, 2009, 100(11), pp. 1529–1535.

[15] X. Xiao, R.W. Hyers, R.K. Wunderlich, H.J. Fecht and D.M. Matson: *Appl. Phys. Lett.*, 2018, 113, 011903.

[16] H. Lamb: *Proc. Lond. Math. Soc.*, 1881, 13.

[17] M. Schick, J. Brillo, I. Egry, and B. Hallstedt: *J. Mater. Sci.*, 2012, 47(23), pp. 81458152.

[18] N. Y. Konstantinova, A. R. Kurochkin, A. V. Borisenko, V. V. Filippov, and P. S. Popel: *Russ. Metall.*, 2016, 2016(2), pp. 144–149.

[19] Wunderlich, R. K. and Mohr, M.: *High Temp.-High Pressures*, 2019, 48, pp. 253-277.

[20] Henein H., Bogno A.-A., Hearn W. and Valloton J.: *J. Phase Equilib. Diffus.*, 2020, 41(6), pp. 784–792.

[21] M. Bedel, G. Reinhart, A.-A. Bogno, C.-A. J. S. Gandin, E. Boller, H. Nguyen-Thi and H. Henein, *Acta Mater.*, 2015, 89, pp. 234-246.

[22] Valloton, J., Bogno, A.-A., Rappaz, M., Henein: *Metall. Mater. Trans. A*, 2022, 53(2), pp. 460-469